

**SPECIAL FEATURE:  
TUTORIAL**

# Laser mass spectrometry for environmental and industrial chemical trace analysis

**Ulrich Boesl\***

Institut für Physikalische und Theoretische Chemie, Technische Universität München, Lichtenbergstrasse 4, 85748 Garching, Germany

**Resonant laser mass spectrometry is a promising method for chemical trace analysis since it combines selectivity, sensitivity and rapidity of measurement. It is a two-dimensional technique incorporating medium- or high-resolution UV spectroscopy and time-of-flight mass spectrometry. No sample preparation and chemical clean-up is necessary to reach detection limits in the sub-ppb range even when highly complicated mixtures of chemical species are analyzed. After an introduction to the principles of resonant laser mass spectrometry, illustrative examples of applications are presented. Drawbacks, possibilities of overcoming them, some interesting features and future developments of resonant laser mass spectrometry are discussed. Copyright © 2000 John Wiley & Sons, Ltd.**

KEYWORDS: laser mass spectrometry; environmental analysis; industrial analysis; trace analysis

## INTRODUCTION

Emissions of many different pollutants caused by mankind disturb or even destroy the atmosphere of our planet. Problems such as the ozone hole, greenhouse effect, acidic rain and high ozone concentrations in the troposphere are the consequences. Many trace pollutants are emitted by combustion processes taking place in motorized vehicles or industrial incinerators. They contribute to the smog in cities and the sunlight-driven chemical formation of ozone or are harmful to humans in themselves. These compounds differ strongly in toxicity (e.g. the isomeric compounds harmless perylene and carcinogenic benzo[*a*]pyrene) and in concentrations.

In view of increasing environmental problems, efficient countermeasures have to be developed and have been started already to reduce the emission of air pollutants (quite apart from problems in water and soil). Thus, the gas cleaning in modern waste incinerators is performed in units which are considerably larger than the combustion kilns themselves and are responsible for the major part of the permanent costs of the incinerator. On the other hand, besides catalytic converters, low-emission vehicles are going to be developed to cope with the air pollution problem. However, for further technological developments in this field, be it for better control of industrial combustion processes (and thus a reduction in gas cleaning efforts), for more efficient catalytic converters (e.g.

for diesel engines) or a more efficient electronic control system for combustion engines, the appropriate analytical tool is necessary in any case.

One of the most promising methods for trace air pollutant analysis is resonant laser mass spectrometry. It combines selectivity, sensitivity and rapidity of measurement. In the following sections, its principles and examples of applications are described. These examples comprise the evaluation of maximum sensitivity of the method, the study of molecular traces of motor oil in the exhaust of motor cars, the measurement of polycyclic aromatic compounds in aerosols and the study of the possibilities of measuring chlorinated dioxins on-line via chemical precursors by on-site experiments in the flue gas of industrial incinerators.

For a general introduction to the application of lasers in mass spectrometry, see Refs 1–4. More information concerning the multiphoton ionization process can be found in Refs 5–8 and in early publications.<sup>9–14</sup> Reviews on resonant laser mass spectrometry are available.<sup>1,2,6,15–21</sup>

## PRINCIPLES OF RESONANT LASER MASS SPECTROMETRY

Resonant laser mass spectrometry (MS) is the combination of two analytical tools, gas-phase UV spectroscopy and mass spectrometry (in particular time-of-flight mass spectrometry). Resonance-enhanced multiphoton ionization (REMPI) represents the linking element and gives rise to the two-dimensionality of resonant laser MS with the parameters mass and UV wavelength. Therefore, this discussion is separated into sections on spectroscopic aspects,

\* Correspondence to: U. Boesl, Institut für Physikalische und Theoretische Chemie, Technische Universität München, Lichtenbergstrasse 4, 85748 Garching, Germany.  
E-mail: ulrich.boesl@ch.tum.de

multiphoton ionization principles, and time-of-flight mass spectrometric considerations.

### Aspects of gas-phase UV spectroscopy

The wavelength range of UV spectroscopy is determined by the energy of the electronic states involved in the absorption process. In general, these electronic states are similar for molecular species of one 'molecular class' such as alkanes, alkenes, alkynes, alcohols, aromatic compounds, aldehydes and so on. Some typical absorption ranges and UV spectra are shown in Fig. 1. Thus, the first (i.e. long-wavelength) absorption bands of aromatic compounds lie in the range from 260 nm (alkylated benzenes) to 350 nm (polycyclic aromatic compounds (PAMs)) while those of aldehydes are to be found in the range from 300 nm to even longer wavelengths. These wavelength ranges are particularly well attainable with tunable lasers. In contrast to larger molecules, many small (in particular two-, three- and four-atomic) molecules show a large enough separation of vibronic bands to be selectively excited even by medium-resolution UV radiation (medium resolution:  $1\text{--}10\text{ cm}^{-1}$ ). For a general introduction to analytical UV spectroscopy, see Ref. 22.

Using lasers, the question rises of how to access the different energy ranges by laser wavelengths. While tunable laser wavelengths are available down to about 370 nm, frequency doubling by non-linear optics is necessary to access the wavelength range down to about 200 nm. Beyond this limit multiphoton absorption (mostly two- or three-photon absorption) spectroscopy has to be involved. For an overview, these details (laser light source, wavelength range and classes of absorbing molecules etc.)

are presented in Fig. 1 together with typical medium-resolution laser UV spectra of some alkylated benzenes and aldehydes.

For some special problems of trace analysis, medium-resolution spectroscopy is not sufficient, even for two-dimensional resonant laser mass spectrometry. One important example is the analysis of structural isomers (e.g. the harmful benzo[*a*]pyrene and the harmless perylene, both with mass 252 u). In principle, the vibrational fine structure of gas-phase UV spectra would allow this distinction in many cases, since it has a similar fingerprint quality to IR spectroscopy. Unfortunately, at room temperature many rotational and some low-frequency vibrational levels are excited in the electronic ground state. This gives rise to congestion of overlapping absorption bands with similar energy and thus a loss of spectroscopic fine structure. As a result, the high selectivity possible for large molecules will be frustrated. To cope with this problem, molecular cooling in supersonic gas beams may be applied. With this technique, 'rotational temperatures' of a few kelvin can be achieved while isolated molecules (condensation can be avoided) are still present. This cooling effect is illustrated in Fig. 2 for the case of monochlorinated anthracene. A single vibronic band has been excited which exhibits large 'rotational broadening' at room temperature and a substantial narrowing for the same band in a supersonic beam. This spectral narrowing now allows isomeric separation, in favorable cases even the separation of isotopomers where isotopes (e.g.  $^{13}\text{C}$ ) are substituted at chemically different positions of the molecule. For more information about molecular spectroscopy in supersonic beams, see Refs 23–25.

To summarize the UV spectroscopic aspects, for most cases where resonant laser MS may be applied in real

UV-Spectroscopy in the Gas Phase:  
Medium resolution

light source	wavelength range	absorbing molecules
Two-photon absorption $\lambda_{\text{EXC}} = 1/2 \lambda_{\text{UV}}$	150 nm	vacuum UV alkanes
	200 nm	alkenes alkynes alcohols
	250 nm	HCN NH <sub>3</sub> OCS H <sub>2</sub> S
frequency-doubling $\lambda_{\text{EXC}} = 1/2 \lambda_{\text{LASER}}$	300 nm	UV aromatic compounds
	350 nm	
tunable laser wavelength $\lambda_{\text{EXC}} = \lambda_{\text{LASER}}$	400 nm	aldehydes
	450 nm	SO <sub>2</sub>
	500 nm	VIS NO <sub>2</sub>

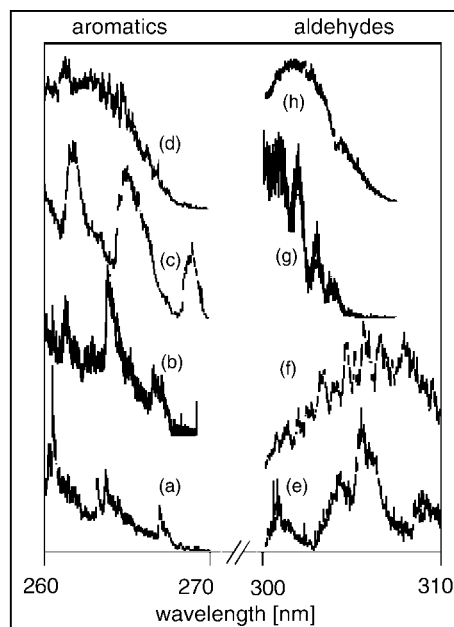


**Figure 1.** UV spectroscopy in the gas phase: medium resolution. Wavelength ranges of absorption are indicated for several types of molecules and for some small molecules. In the row 'light source,' the way to reach these wavelength ranges by laser light is indicated. In addition, medium-resolution gas-phase UV spectra are shown for the aromatic compounds toluene (a), *p*-xylene (b), ethylbenzene (c) and 1,3,5-trimethylbenzene (d), and for the aldehydes formaldehyde (e), acetaldehyde (f), acrolein (g) and propionaldehyde (h). These spectra were measured in an effusive molecular beam at room temperature by multiphoton ionization spectroscopy (instead of UV absorption the ion current is recorded as a function of laser wavelength at a fixed mass; in other words, these spectra represent mass-selected UV spectra).

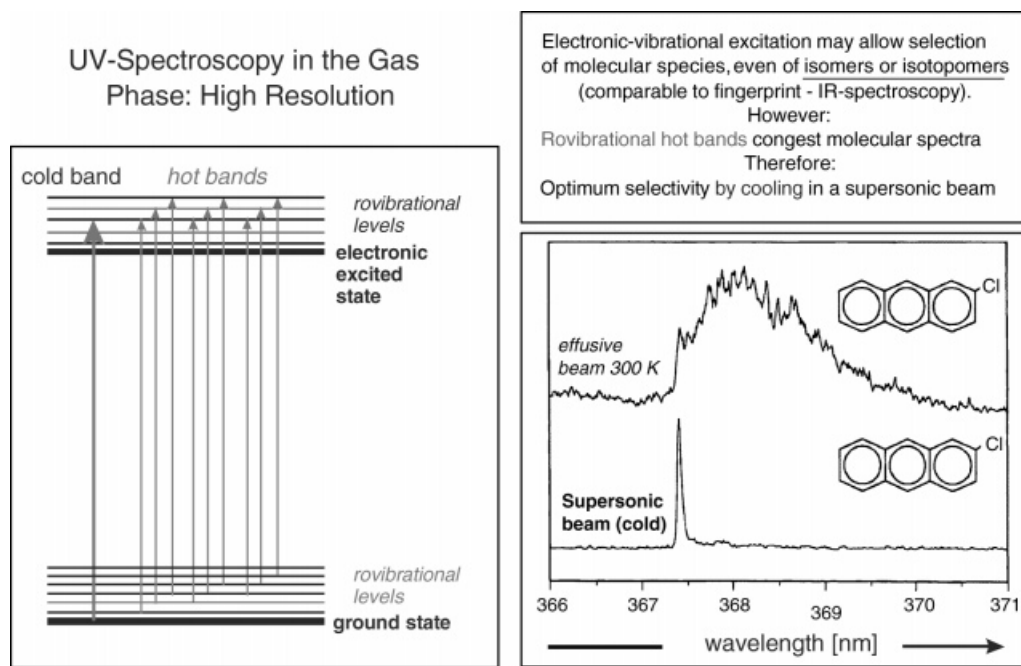


**Figure 2.** UV spectroscopy in the gas phase: high resolution. At room temperature many rovibrational levels (vibrational levels with their rotational sublevels) are excited in the ground state. This results in the congestion of the UV spectrum due to vibrational hot bands. In addition, many rotational sublevels of vibrations in the ground state cause a broadening of single vibrational bands since the number of allowed rotational transitions increases considerably. In the schematics on the left, transitions are indicated by arrows which cause vibrational hot bands at a similar wavelength as the cold band; this would give rise to overlapping bands in a hypothetical UV spectrum. The two spectra of chloroanthracene illustrate the effect of rotational broadening: the vibronic band at 367.4 nm is rotationally broadened in the effusive beam. Cooling of internal molecular degrees of freedom (rotation, vibration) in a supersonic beam results in a very narrow line allowing high-resolution gas-phase UV spectroscopy to be performed by varying  $\lambda_{\text{exc}}$ .

practical problems, medium resolution (i.e.  $\Delta\nu =$  a few  $\text{cm}^{-1}$ , room temperature molecular beam) is sufficient. For special problems, high-resolution (i.e.  $\Delta\nu < 0.1 \text{ cm}^{-1}$ , supersonic beam cooling) UV spectroscopy supplies the necessary selectivity. In other words, in most cases less sophisticated laser gas inlet and vacuum systems are sufficient for trace pollutant analysis with the favorable result of a more practical, user-friendly and even mobile analytical instrument.

### Resonance-enhanced multiphoton ionization

The spectroscopic features discussed above can be utilized in a ionization process via resonance-enhanced multiphoton ionization. In the case of the most favorable (1 + 1) ionization, the first photon is absorbed into an excited electronic state. This state acts as an intermediate state for the multiphoton ionization process; its excitation is subject to more or less sharp resonance conditions depending on the structure of its gas phase UV spectrum (narrow lines for cold molecules, broad ones for hot molecules as discussed above). Only when the resonance conditions for the first (spectroscopic) absorption step are fulfilled and selective excitation takes place can a second photon be absorbed up to the ionization continuum with adequate efficiency. Resonance-enhanced and therefore species-selective multiphoton ionization, applied to a mixture of gases located in the electric field between two electrodes, therefore results in a species-selective ion source.

This whole scheme of ionization is illustrated in Fig. 3, where, in addition, on the right-hand side an example

demonstrates the possibilities and quality of this selective ion source. Two gas chromatographic spectra are shown, which are part of a measurement made in the gas phase above a gasoline sample. They represent the four isomeric species ethylbenzene and *p*-, *m*- and *o*-xylene, all of them with the molecular mass 106 u. Conventional mass spectrometry would not be able to separate these isomeric components. In the fast, medium-resolution gas chromatograph used here, *p*- and *m*-xylene also could not be separated. The upper gas chromatogram shows all four compounds detected by non-selective electron ionization in a mass spectrometer set to monitor mass 106 u. The lower gas chromatogram shows a single GC peak due to *p*-xylene obtained by (1 + 1) multiphoton ionization at 272.34 nm. This wavelength is resonant with a vibronic band of *p*-xylene only. UV spectroscopy employing molecular cooling in a supersonic beam necessary for this high selectivity was achieved by a special coupling of GC column and supersonic beam valve.<sup>26</sup>

In Fig. 4, an estimation of the sensitivity for (1 + 1) ionization is given. Non-saturation of the first absorption step is assumed ( $\sigma_1 I \tau \ll 1$ , where  $\sigma_1$  is the absorption cross-section,  $I$  the laser intensity and  $\tau$  the laser pulse length), and also typical cross sections  $\sigma_1$  for  $S_0 \leftarrow S_1$  absorption of aromatic compounds and  $\sigma_2$  for absorption to the ionization continuum. Finally focusing a 100  $\mu\text{J}$  laser pulse (10 ns pulse length) on to a spot of 0.1  $\text{mm}^2$  gives a very reasonable laser power of  $10^7 \text{ W cm}^{-2}$ . Under these conditions, 10% of all neutral molecules within the ionization volume (i.e. cross-section of laser and molecular beam, in Fig. 4 the ionization volume  $V$  is 0.1  $\text{mm}^3$ ) are ionized. This is equivalent to a detection

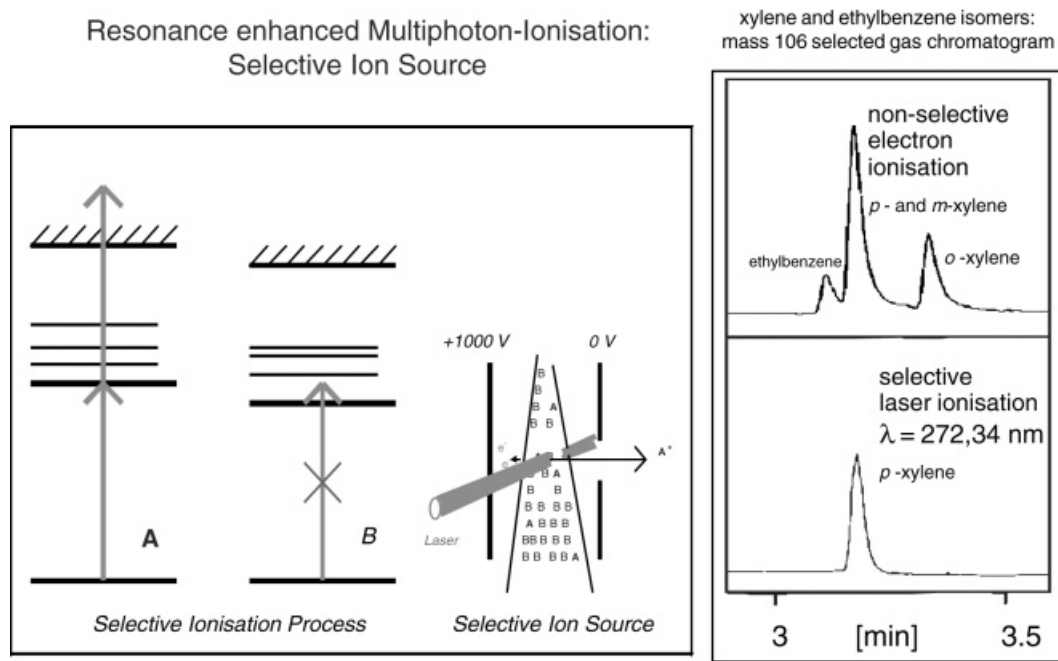


**Figure 3.** The selectivity of resonance-enhanced multiphoton ionization: principle of excitation and ion source, and illustrative spectra. Resonance-enhanced multiphoton ionization is a two-step absorption process. The first absorption step (usually a one-photon process) involves gas-phase UV spectroscopy. If the wavelength of the exciting laser is in resonance with a molecular transition (e.g. molecule **A**, but not molecule **B**), a second photon may be absorbed into the ionization continuum. If this process takes place within an electric field, an ion beam will be generated which only contains molecular ions **A**<sup>+</sup> (highly selective ion source). On the right side two gas chromatograms of the same sample recorded mass selectively in a time-of-flight mass analyzer are shown. Two different ionization techniques were used: non-selective electron ionization and highly selective laser ionization. In the first case, the four isomers of mass 106 appear, whereas in the second case *p*-xylene is detected selectively (for separation of structural isomers, high-resolution UV excitation is necessary, as shown in Fig. 2).

### Resonant Multiphoton Ionisation: Estimation of Sensitivity

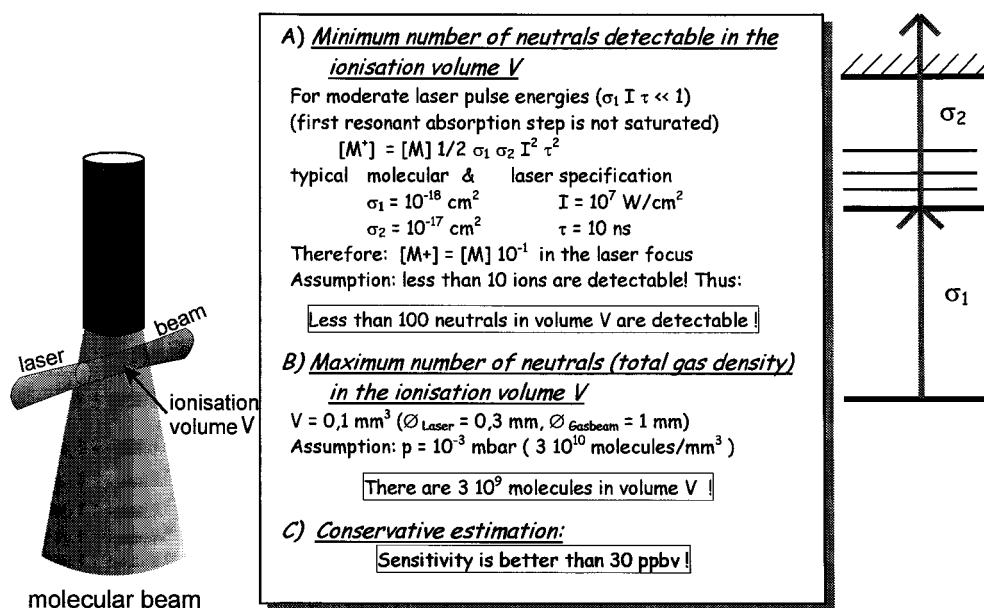


**Figure 4.** Estimation of the sensitivity of resonance-enhanced multiphoton ionization. This is a conservative estimation assuming a  $100 \mu\text{J}$  laser pulse energy, a pressure of  $10^{-3}$  mbar in the ionization volume and a small absorption cross-section for the first step. Enhancement by three orders of magnitude is possible by using more powerful lasers and higher gas densities in the molecular beam.

limit of 100 neutral molecules in the ionization volume if fewer than 10 ions formed in the ion source are detectable. Finally, assuming a pressure of  $10^{-3}$  mbar in the molecular beam (which is easily achievable in a

continuous effusive beam with a vacuum chamber pressure kept below  $10^{-5}$  mbar by a  $150 \text{ l s}^{-1}$  vacuum pump) gives a total number of  $3 \times 10^9$  neutral molecules present in the ionization volume. In other words, fewer than 100

molecules of one species within  $3 \times 10^9$  molecules of the gas sample are detectable, corresponding to a sensitivity of better than 30 ppbv.

This is still a fairly conservative estimation. An improvement by three orders of magnitude is possible in many cases: A laser pulse energy of 1 mJ (same intensity, but a cross-section of 1 mm) still is reasonable; a pressure of  $10^{-2}$  mbar in the molecular beam should be possible without loading the vacuum system too heavily; a value of  $10^{-18}$  cm<sup>2</sup> for the cross-section of the first absorption step is a fairly small value and may be larger in many cases. All these changes will improve the sensitivity to a level below 100 pptv. Recent experiments confirmed this value. For naphthalene with a concentration of 15 pptv, an ion signal has been detected at a signal-to-noise ratio of 2.<sup>27</sup> A high linearity of the ion signal versus concentration in the range  $10^4$ – $10^{-2}$  ppbv was measured. Others have reported the detection of 45 pptv of naphthalene at a signal-to-noise ratio of 20.<sup>28</sup> Furthermore, in a realistic gas mixture due to emission from an incinerator plant, a naphthalene concentration of 2 ppbv has been detected at a signal-to-noise ratio of better than 10.<sup>29</sup> Even an increase in the naphthalene concentration from below 50 to 100 pptv during a change of the combustion process within the incinerator could be resolved.

### Time-of-flight mass spectrometry

Time-of-flight mass spectrometry is probably the easiest way of analyzing the mass of ions (for a review, see Refs 30 and 31; see also Refs 32–34). Being a repetitive, pulsed technique, it is optimally adapted to pulsed ion sources such as pulsed laser ionization. There, ions are formed in short time intervals (during laser pulses of typically  $10^{-8}$  s) and in a well defined spot (laser focus). The former guarantees a nearly equal starting time of all ions, the latter a very similar potential energy within the static electric field of the ion source. After ionization, all ions are instantly accelerated into the field-free drift region. During acceleration, potential energy is transformed into kinetic energy which is again similar for all ions. As  $E_{\text{pot}} = E_{\text{kin}} = 1/2mv^2 = \text{constant}$ , masses  $m$  and flight times  $t$  show a well-defined proportionality:  $t \approx \sqrt{m}$ . In practice, there is a constant contribution to the flight time (e.g. due to delay times in electronic devices). Thus with the equation  $t = a + b\sqrt{m}$ , time-of-flight mass spectra may be described;  $a$  and  $b$  can be determined for fixed conditions (e.g. voltages in the ion source) by measuring flight times for two different ions of known masses.

Unfortunately, small spreads of the initial energy of ions reduce the mass resolution of linear time-of-flight mass analyzers significantly. Sources of initial energy are the finite width of the laser beam producing ions at points with different potentials, initial velocity spread of the primary neutrals, kinetic energy release during fragmentation or space-charge effects due to high ion density numbers. The last effect is particularly unfavorable since it is a dynamic effect which may induce not only large initial energies but also large shifts on the time domain.<sup>32,34</sup> All these effects can be reduced by positioning the ion detector at a point called the space-focus. The space-focus is a particular feature of pulsed ion sources. It is a point in the field-free drift region where those ions which are formed further away from the attracting electrodes of the ion

source (and therefore have higher kinetic energy) overtake those formed nearer to the attracting electrode (and thus have smaller kinetic energy). However, even this counter measure (ion detection in the space-focus) does not allow a mass resolution of better than about  $R_{50\%} = 1000$  for a drift length of about 1 m, and space-charge effects may even push the mass resolution below  $R_{50\%} = 200$ . In particular in trace analysis, so many different species are present in a single sample that despite the more or less selective ionization large ion density numbers cannot be avoided. Although mass analysis would allow the separation even of a large manifold of ionic species, space charge will simply reduce this ability or make it impossible.

The use of reflectron time-of-flight mass analyzers can solve this problem, since they compensate for most of the initial ion energy spread as long as this does not exceed about 20% of the total ion energy. This compensation is achieved by reflecting all ions in a relatively weak electric field. Owing to their larger energy, fast ions penetrate deeper into this reflecting field and therefore need more time to turn around than slow ions of the same mass. By choosing the right slope of this weak reflecting field, the point where fast ions overtake the slow ones a second time (second space-focus) may just be positioned at the surface of the ion detector. While the ion source now can be designed for minimized space-charge effects (e.g. by using high electric fields due to small distances between repelling and attracting electrodes), the drift region and the ion reflector are solely responsible for the compensation of the initial ion energy spreads. Figure 5 shows the scheme of a reflectron (top) and the molecular ion mass region of benzene (bottom), measured once with a linear and once with a reflectron time-of-flight mass analyzer (the same instrument was used with identical ion source conditions but changed potentials of the reflecting field). The change in mass resolution is evident. The routine reflectron mass resolution  $R_{50\%}$  is 2000–3000, whereas that of linear-type instruments is 10 times smaller. In addition to the considerably improved mass resolution, reflectrons supply better signal-to-noise ratios: on the one hand, in reflectrons, the ion mass peak intensities are larger at the same integrated intensity per mass, and on the other, narrower time gates can be used for single mass recording which reduces the contribution of background ions; these are distributed over a large time, or mass range. For further details on time-of-flight mass spectrometers, see Refs 31–34.

---

## APPLICATIONS OF RESONANT LASER MASS SPECTROMETRY IN TRACE ANALYSIS

---

### Detection limit in realistic gas mixtures

In Fig. 6, some results are presented for an experiment performed to determine the detection limits of resonant laser MS of trace compounds in realistic gas mixtures.<sup>35</sup> For this purpose, a special gas mixture was used consisting of 96% of N<sub>2</sub>, 2.4% of motor car exhaust gases and 17 different, mostly chlorinated, hydrocarbons with a relative concentration of about 0.1% of each component. To this 'soup,' 93 ppbv of aniline were added.

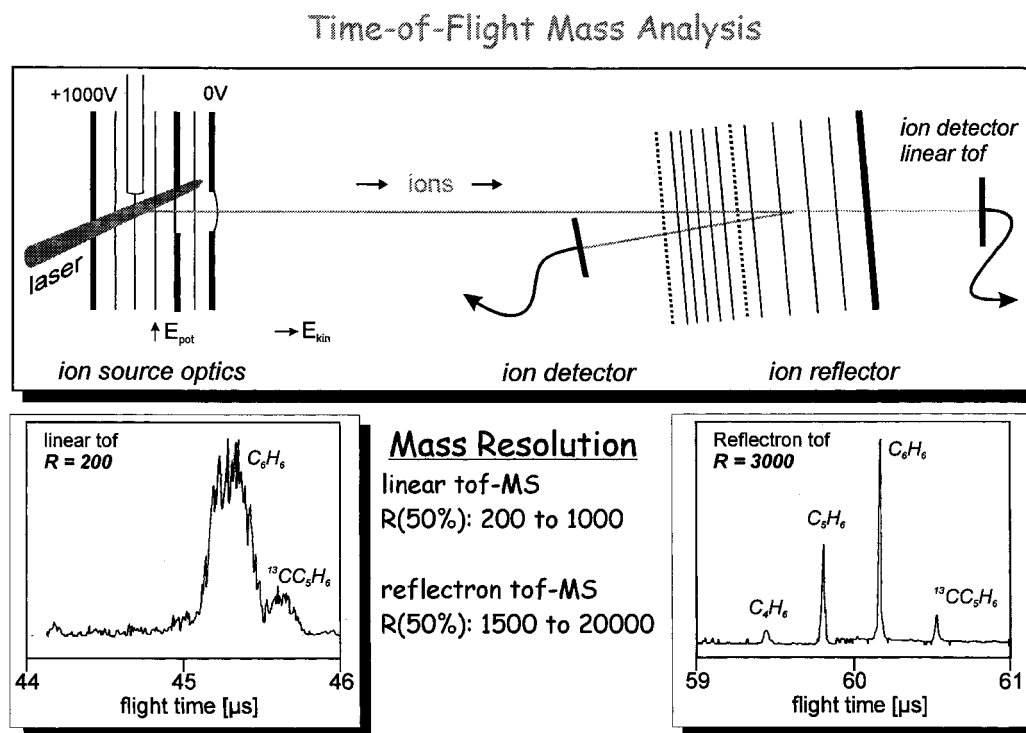


**Figure 5.** Schematic of a reflectron time-of-flight mass spectrometer consisting of a double-stage ion source, a field-free drift region, an ion reflector and an ion detector (the thin lines symbolize equipotential lines of electric fields). The ion reflector is able to compensate for the effect of a spread of the ion energy of up to  $\pm 10\%$ . In a linear time-of-flight mass analyzer (represented by the same scheme without ion reflector, but with elongated field-free drift region and ion detector at its end) this leads to strong reduction of mass resolution. This is illustrated with two mass spectra measured in the same instrument, which could be switched from reflectron to linear mode.

The comparison of the corresponding ion signal and the background signal then allows an estimate of the minimum concentration of aniline which still gives an ion signal with a signal-to-noise ratio of 3 and thus the detection limit. This experiment<sup>35</sup> was chosen to illustrate the detection limits of resonant laser MS, since here the problems of interfering abundant components have been considered in a very defined way. On the other hand, high-resolution excitation by laser UV radiation and a supersonic beam has been involved. Others have reached considerably lower detection limits down to the low ppt range,<sup>27–29</sup> but either without use of appropriate laser wavelengths or supersonic beams for high-resolution excitation, or only in simple gas mixtures of pollutant and carrier gas.

In this experiment, a supersonic beam was used, the laser wavelength was tuned to 293.8 nm, where aniline shows a vibronic band, and a set of so-called 'off/on/off' scans were made, where the molecular beam was blocked, unblocked and blocked again to measure the background signal before and after ionization within the beam. The result is shown in Fig. 6 at the top. The dotted line shows the background signal with no sample flowing in on a 100-times magnified intensity scale. From the r.m.s. baseline and the 93 ppbv aniline ion signal, a detection limit of 540 pptv ( $S/N = 3$ ) was deduced, which is in good agreement with the value of 450 pptv found from a different experiment with aniline seeded in a helium carrier gas. Although this is an extrapolated and not an actual detection limit, this value is more likely an upper than a lower limit. As mentioned above, naphthalene with concentrations in the low-pptv range has been

detected by resonant laser MS. On the other hand, high linearity of the ion signal versus concentration has been measured over five orders of magnitude and down to 100 pptv.<sup>27,28</sup>

Further tests (laser spectra and mass spectra) were performed to prove that contributions from other highly abundant components (with concentrations of 1000 ppmv) did not produce ion signals distinguishable from the background signal and thus would not interfere with the ion signal of aniline at a concentration of 500 pptv.<sup>35</sup> In Fig. 6, at the bottom, sections of two resonant laser mass spectra are shown, the first of a mixture of  $N_2$  and 93 ppbv aniline, the other of the 'soup,' described above, and the same amount of aniline (dotted line). The ion signals are very similar (the difference in height is within the experimental error) and no other signal or change in the ion peak shape was observed. The same result (i.e. no interference) is found for the mass-selected laser spectra of both mixtures. Mass-selected laser spectra are measured by recording only the ion signal within a time gate set at the mass of the ions of interest as a function of the laser wavelength. This is clear evidence that in the case of the soup–aniline mixture [dotted line in Fig. 6(b)], no interference with other gas components is occurring despite the large number of similar components present in the soup. Similar experiments were performed for eight target species whose concentrations were below 100 ppbv while all other components in the mixture which could possibly interfere were present at typically 1000 ppm. This indicates sub-ppb detection limits for all of these components.

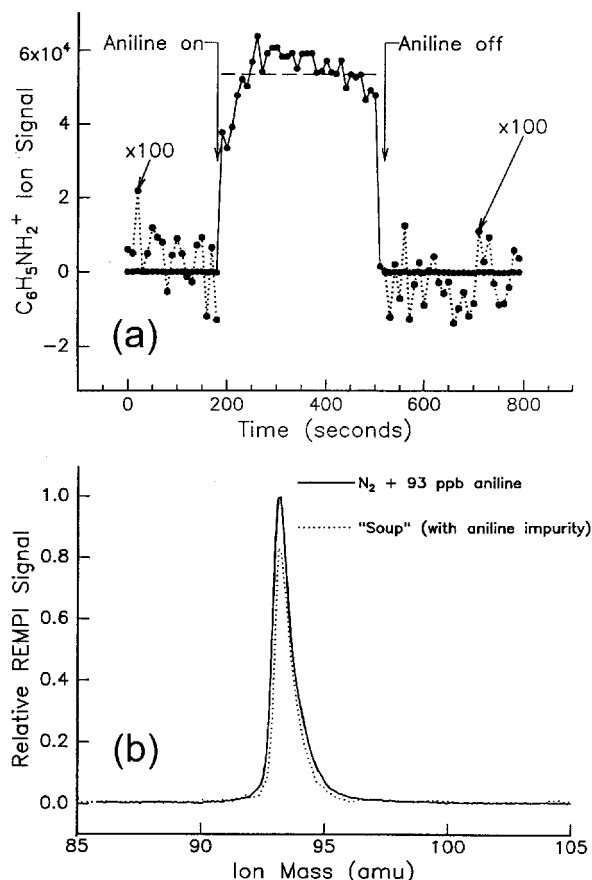


**Figure 6.** Determination of the sensitivity of resonance-enhanced multiphoton ionization: off-on-off switching of a molecular beam due to a complicated gas mixture (soup) with 93 ppb of aniline after aniline-selective laser ionization (a) and mass spectrum with aniline-selective laser ionization of nitrogen seeded with 93 ppbv of aniline and of the complex mixture with 93 ppbv of aniline (b). Comparison of background (off-signal) and aniline (on-signal) gives a detection limit (signal-to-noise ratio of 3) of 540 pptv of aniline in the complex mixture. Reprinted from T. N. Tanada, J. Velazquez, N. Hemmi, T. Cool, *Ber. Bunsen-Ges. Phys. Chem.* **97**, 1516–1527 (1993) with permission of Wiley-VCH, Weinheim.

### Detection of traces of motor oil in the exhaust of motor cars

The detection of motor oil in the exhaust of combustion engines is of interest for several reasons. On the one hand, such experiments may provide information about oil consumption mechanisms, or even allow the fast determination of oil components; on the other hand large PAHs (which mostly are due to motor oil) may degrade the surface of electrochemical sensors which allow one to monitor the oxygen content of exhaust gas in motor cars. These sensors are needed to control the oxygen concentration for optimum catalytic converter efficiency. To discriminate PAHs from gasoline and from motor oil, laser MS has been applied to the exhaust of a hydrogen motor (same engine as for gasoline with only minor changes) at a BMW test facility.<sup>36,37</sup> The total PAH content in the exhaust due to motor oil was found to be in the 1 ppmv range. The resonant laser mass spectrum of these PAH is shown in Fig. 7(a). In this mass spectrum more than 15 peaks with a signal-to-noise ratio of better than 10 contribute to the total of 1 ppmv. This indicates a sensitivity

of better than 10 ppbv of single molecular components despite the high speed of measurement. Mass spectra such as those in Fig. 7(a) are achievable at single laser shots, in principle. For a reasonable laser repetition rate of 20 Hz, this would mean that dynamic motor processes can be monitored by mass spectrometry with a time resolution of 50 ms. For reasons of better absolute accuracy, averaging over 50–100 laser shots is usual, however.

Comparison of gasoline and hydrogen motor experiments allowed the assignment of the high-mass peaks to motor oil components. In Fig. 7(a), at the top, a small part of the high-mass range of a mass spectrum measured

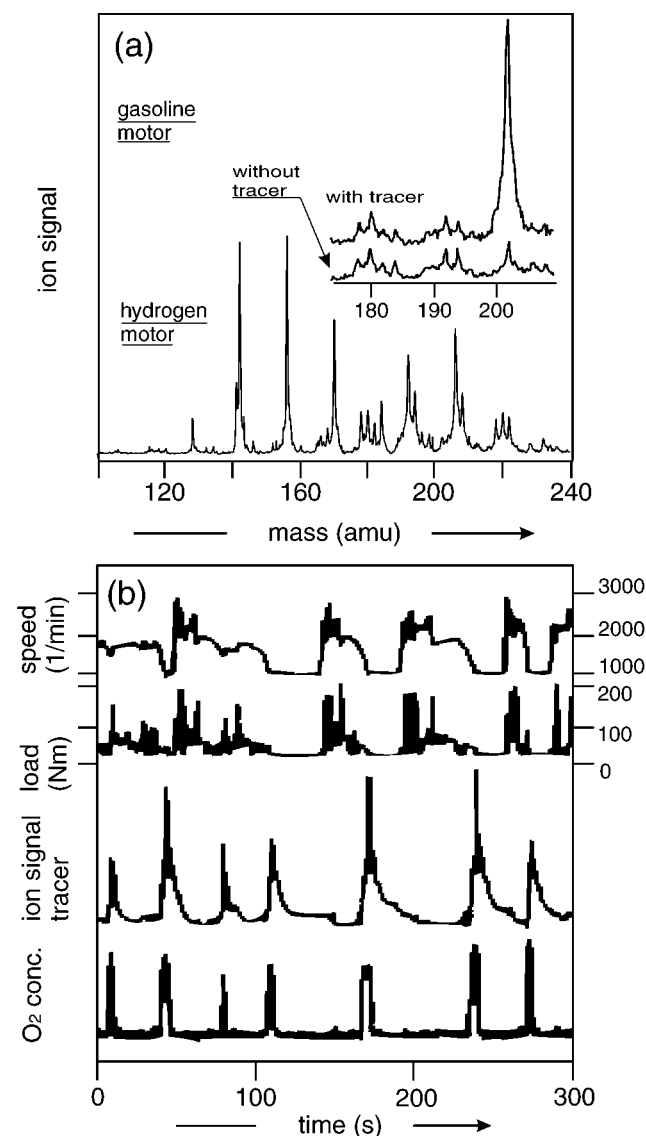


**Figure 7.** Traces of motor oil in exhaust gas. (a) Mass spectrum of PAHs in the exhaust of a hydrogen fueled motor (motor oil is the only source of PAHs) and two mass spectra (reduced sensitivity of ion detector) of a gasoline-fueled motor: one measured without tracer and one with 1% of tracer (pyrene at mass 202) in the motor oil. (b) The tracer signal as a function of speed and load during a test drive of a car. Fast dynamic changes of the tracer (pyrene) signal indicate a highly dynamic variation of motor oil consumption. (c) Quantitative motor oil consumption as a function of speed and load. The decrease above  $5500 \text{ l min}^{-1}$  is due to destruction of the tracer (high combustion temperature). The modulations are due to changing thickness of the motor oil film at the inner walls of the cylinder. See also Refs 36 and 37.

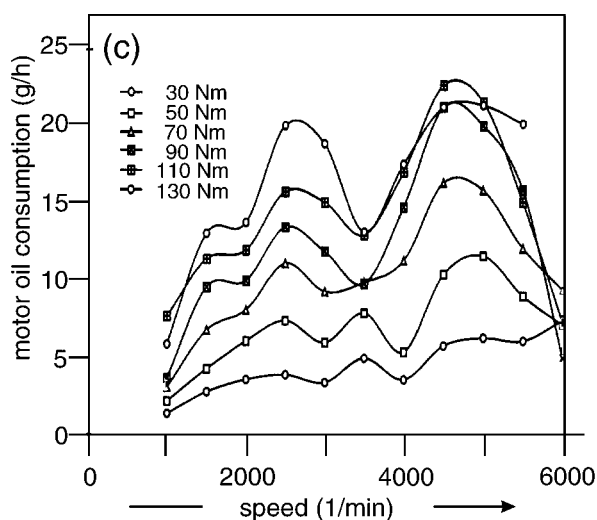


Figure 7. (continued).

in the exhaust of a gasoline engine is shown (the mass resolution is reduced owing to the use of a linear time-of-flight mass analyzer; see space-charge effects discussed above). Whereas the lower trace shows a mass spectrum without addition of a molecular tracer to the motor oil, the upper trace is due to the addition of 1% of pyrene, which resulted in a significant peak at mass 202. This peak was stable for many hours, indicating that the concentration of pyrene in the motor oil was not rapidly reduced owing to strong evaporation. Pyrene was one of several possible species considered as tracer molecules. One advantage of pyrene is its low cost. In addition, it can be ionized efficiently with a wavelength of 266 nm, the fourth harmonic of an Nd:YAG laser.

Comparison of the pyrene mass peak with conventional hydrocarbon analysis under various, stationary motor conditions resulted in the following conclusions: (i) most motor oil loss is due to evaporation within the combustion chamber (i.e. the cylinder of the engine); (ii) nearly 90% of the evaporated oil components stay unburned and are found as such in the exhaust (this amount decreases in extreme situations such as at high speed above 5500 rpm); (iii) consequently, the concentration of a tracer (e.g. pyrene) is a reliable measure of the overall oil consumption. Two different applications of pyrene as a tracer in motor oil are also shown in Fig. 7. One displays fast dynamic effects of oil consumption [Fig. 7(b)] and the other represents measurements at different stationary motor conditions and allows a speed-load mapping of oil consumption [Fig. 7(c)]. Figure 7(b) shows four signals as a function of time: (i) the speed between 1000 and 3000 rpm, (ii) the load between 20 and 200 Nm, (iii) the tracer signal and (iv) the relative oxygen concentration. It can be clearly seen that high motor oil consumption occurs when both speed and load have decreased rapidly from a high level to a minimum value, which is correlated with a strong decrease in the combustion process. These short moments of reduction of thrust force are characterized by sharp oxygen peaks. The sharp increase in motor oil consumption at these times can be explained by a sudden pressure reduction in the cylinder inducing enhanced evaporation of oil components from the walls within the cylinder. The oil consumption measurements have not yet

been quantified, since at the moment no adequate methods exist to measure the total mass flow of the exhaust with 50 Hz time resolution. Nevertheless, even qualitative results about highly dynamic oil consumption may be very valuable for engineers developing modern combustion engines.

The results in Fig. 7(c) differ from those in Fig. 7(b) in several respects. Now the motor operates under stationary conditions, each of which is characterized by a pair of values of speed and load and which are kept constant for several minutes. The motor oil consumption is measured for each of these stationary conditions and could now be quantified (given in  $\text{g h}^{-1}$ ). For different speeds and constant load, a curve of oil consumption could be measured. Varying the load resulted in groups of oil consumption curves. Instead of a smooth, steady increase in oil consumption with speed (which one might expect), these curves show a more or less periodic modulation of oil consumption. One explanation is that the piston rings not only move with the piston but also are subject to secondary forces resulting in rotation and twisting. This influences the function of the piston ring as a scraper of the oil and finally leads to a varying thickness of the oil film at the inner walls of the cylinder. Thick films then give rise to an increased amount of evaporated oil and thus an increased motor oil consumption. One should note that the measurement of the whole oil consumption-speed-load map took 1 day with resonant laser mass spectrometry, but takes 1 month or even longer with conventional techniques (e.g. weighing of oil before and after running the motor under stationary motor conditions).

#### Trace analysis of PAHs in aerosols

PAHs in the troposphere are mostly incompletely burnt or even unburned components of all kinds of combustion processes, such as motorized traffic, waste incinerators, industrial production processes, power plants and private heating. Most of these PAHs are not present as free molecular species in the gas phase but are adsorbed on particle surfaces. For environmental analysis of the atmosphere, therefore, not only the gas phase, but also the aerosols have to be investigated. These studies should be species selective, since PAHs differ strongly in toxicity, some being well known as carcinogenics whereas others are more or less harmless. An adequate analytical technique therefore should be outstanding not only in terms of its sensitivity but also in particular in terms of its selectivity. Most conventional techniques therefore include a chemical clean-up to reach this sensitivity. This clean-up procedure is very time consuming and expensive, besides imposing other restrictions. Resonant laser MS combined with laser desorption enables one to study molecular species adsorbed on surfaces with no chemical clean-up being necessary owing to its high (two-dimensional) selectivity. Single samples may now be analyzed within a few minutes. In the measurement presented in Fig. 8, this method was applied to compare the PAH loads of aerosols at different sites.<sup>38</sup>

For laser desorption, a pulsed  $\text{CO}_2$  laser and for ionization a XeCl excimer laser were used. The latter emits at a wavelength of 308 nm, where PAHs absorb. For sampling aerosols in the atmosphere about  $19 \text{ l min}^{-1}$  of air were passed through filter material consisting of quartz fiber for

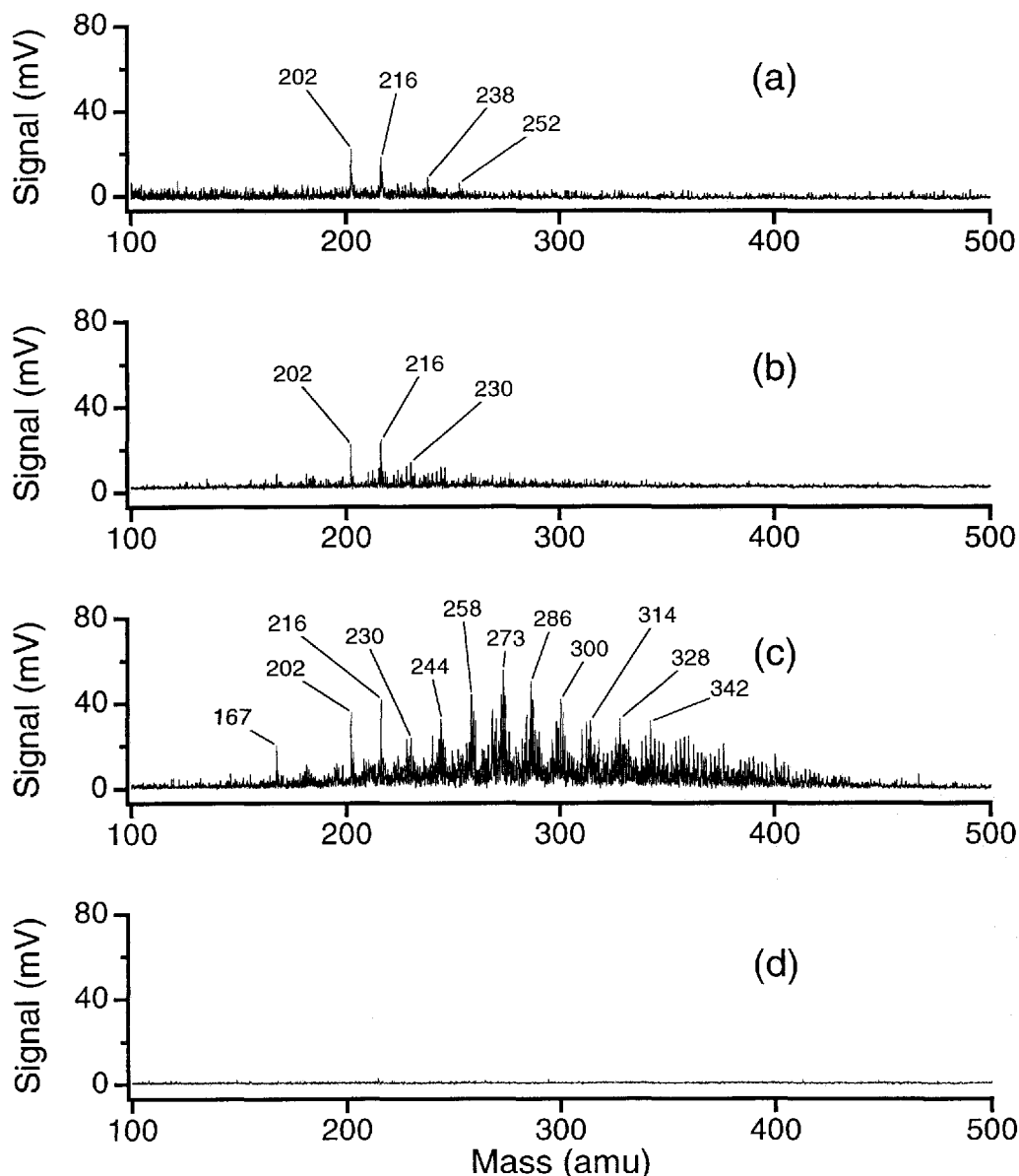


**Figure 8.** Laser desorption laser/post-ionization mass spectra of aerosol samples from different locations: (a) rural site, 100 m from a farmhouse in a harvested field; (b) industrial zone, close to a material recycling plant with only electric power; (c) downtown road, 2 m away from a main road; (d) blank filter. Reprinted from Q. Zhan, P. Voumard, R. Zenobi, *Rapid Commun. Mass Spectrom.* **9**, 119–127 (1995) with permission of John Wiley & Sons, Chichester.

1 h and at a height of 45 cm above the ground. The covered filter was cut, mounted on the tip of a sample holder and introduced into the mass spectrometer through a vacuum interlock. This procedure takes only a few minutes. No additional extraction, purification or preconcentration was performed.

Figure 8 shows the mass spectra of aerosols from three different locations and also that of a blank filter. It is obvious that the spectra for the countryside and the industrial zone show a different range of the most intense mass peaks (namely 200 to 230 u) than the mass spectrum of the downtown road (mass 200–400 u). Also, the integrated signal intensity differs substantially; however, it was not possible to measure the PAH load per aerosol particle. Even the few intense mass peaks in the rural site and industrial zone spectra (i.e. 202, pyrene or fluoranthene; 116, 230, methylated and ethylated mass 202 species) may be explained by aerosol transport over long distances from

regions of high traffic or intense residential heating. Anyway, traffic seems to be one of the main sources of PAHs in aerosols.

We should mention one important difference from other mass spectrometric desorption techniques such as secondary ion mass spectrometry (SIMS), fast atom bombardment (FAB), laser desorption/ionization (LDI) and matrix-assisted laser desorption/ionization (MALDI). In resonant laser ionization performed after laser desorption, ionization and desorption are separated. Therefore, they can be optimized separately and selective ionization is possible; matrix or substrate effects do not play an important role. SIMS, FAB and LDI are mostly not selective enough and often even not 'soft' enough (concerning fragmentation) desorption/ionization techniques to avoid interference of the many different trace compounds of an environmental sample due to the similar masses of molecular or fragment ions. Even ion–molecule reactions in the dense gas

phase of the plume directly above the sample surface after desorption may influence the signal intensity of special trace compounds and falsify quantitative analysis in the case of these desorption/ionization techniques. The missing selectivity of these desorption/ionization techniques can be compensated by tandem MS techniques (as used in post-source decay MS;<sup>39</sup> for an introduction to tandem MS, see also Ref. 40). This works out for analytical purposes if few molecular species are present in a sample. If a highly complicated mixture of hundreds of different species has to be analyzed, time-consuming chemical clean-up and high-resolution GC/MS are necessary which is not compatible with pulsed desorption methods. On the other hand, the high accuracy of quantifying and the low detection limit of this highly sophisticated analytical method is not reached by state-of-the-art laser desorption/ionization mass spectrometry. The benefit of the latter is a high speed of recording mass spectra combined with high selectivity.

### On-line dioxin analysis via chemical precursors

Since the chemical accident in the Italian town Seveso, chlorinated dibenzodioxins (in particular 2,3,7,8-tetrachlorodibenzodioxin) are known to rank among the most poisonous environmental pollutants and a great deal of energy has been expended on the development of adequate trace analysis methods. The main problems in dioxin analysis are the extremely low concentrations and the large number of structural isomers belonging to each group of dioxins with equal numbers of substituted chlorine atoms. For instance, 22 structural isomers of tetrachlorodibenzodioxins exist. The toxicity of these isomers differs by several orders of magnitude. Therefore, only an isomer-selective dioxin analysis is informative enough to study the risks of dioxin. Highly sophisticated techniques (mostly combining GC and high-resolution MS) have been developed with excellent sensitivity and selectivity. Their main restriction, however, is the very time-consuming chemical clean-up procedure which makes any rapid analysis (even on the time-scale of hours) impossible, not to speak about on-line analysis. In many situations, a rapid dioxin analysis is very desirable, e.g. in the case of chemical accidents or for controlling the exhaust of industrial combustion processes.

Resonant laser MS may allow new solutions to this problem. Thus, the separation of dioxin isomers by highly selective UV spectroscopy in supersonic beams could be tried. For some dichlorinated dibenzodioxins this has been demonstrated already, so that there may exist a certain probability of successful selective ionization of dioxin isomers. However, the extremely low concentrations to be detected (the legal limits of dioxin emissions lie in the range of sub-ppq: ppq corresponds to 1 in  $10^{15}$ ) make this solution of the analytical problem very unreasonable for a practical application. On the other hand, several research groups have found good correlations between some chemical precursors and the so-called international toxicity equivalent (I-TEQ) for polychlorinated dibenzodioxins and -furans (PCDD/F). This I-TEQ is an average concentration to which all dioxins weighted by their toxicity contribute. In addition to special highly chlorinated phenol and benzene isomers, it was found recently that monochlorobenzene belongs to these special precursors.<sup>41</sup>

This correlation is shown in Fig. 9 at the top. Note that the precursor concentration is in the pptv range which is about 1000 times larger than that of the chlorinated dioxins.

Owing to this correlation, an experiment has been performed to find out if monochlorobenzene is detectable on-line in the flue gas of a waste incinerator by resonant laser mass spectrometer.<sup>42</sup> The idea behind an on-line trace analysis of the flue gas emitted from the combustion chamber of an incinerator is that a fast on-line pollutant analysis could permit much better (since it is faster) control of the combustion process, thus avoiding pollutants at a very early stage. The experiment was performed with a laser mass spectrometer specially equipped for hot emission gases of an incinerator. The sampling line from the combustion chamber to the ion source was heated to more than 550 K. A quartz filter protected the mass spectrometer from the heavy dust load of the emission gases.

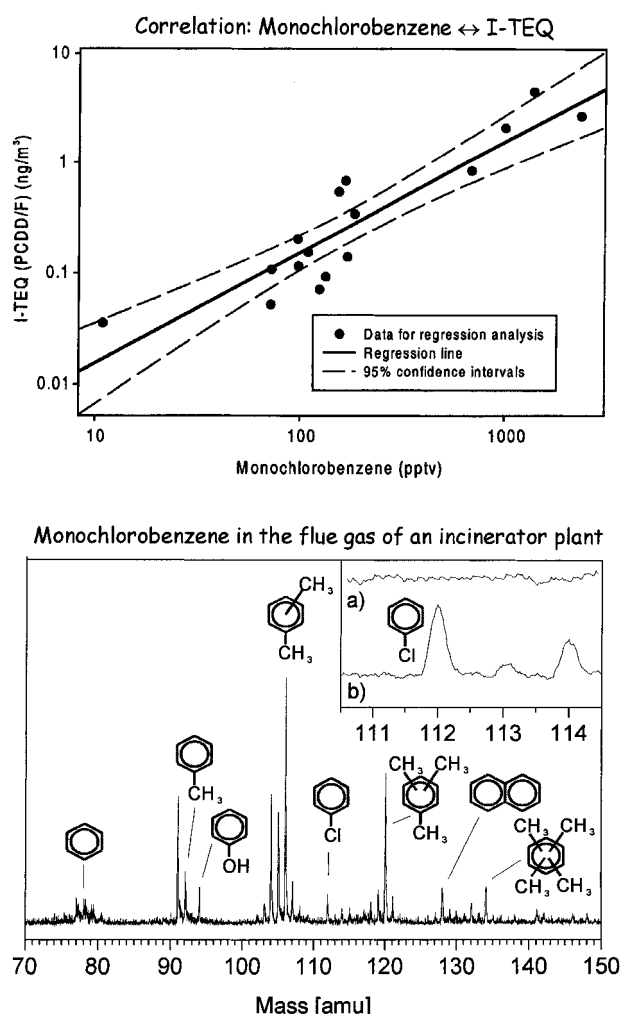


**Figure 9.** Correlation between monochlorobenzene and the international toxicity equivalent of polychlorinated dibenzodioxins and -furans (I-TEQ (PCDD/F)), measured by conventional trace analysis procedure (i.e. sampling, chemical clean-up, high-resolution GC/MS). Regression line and 95% confidence interval are displayed. The correlation coefficient of the measurement is  $r = 0.91$ . Below: resonant laser mass spectrum of the flue gas of a special waste incinerator plant measured at 269.8 nm laser wavelength, revealing PAHs and a monochlorobenzene signal. Inset: part of the mass spectrum measured at 269.8 nm (b) and at 266 nm (a). Reprinted from R. Zimmermann *et al.*, *Rapid Commun. Mass Spectrom.* **13**, 307–314 (1999) with permission of John Wiley & Sons, Chichester.

The whole instrument (containing a tunable laser system, mass spectrometer, power supplies and data acquisition system) was positioned just beside the combustion chamber of a special waste incinerator on a walking metal grid some 20 m above ground. The result of the experiment is shown in Fig. 9(b). The mass spectrum was taken with a laser wavelength of 269.8 nm, where monochlorobenzene has a resonance and is ionized particularly efficiently. In fact, a distinct ion signal is observed at the mass 112 of chlorobenzene in the midst of many considerably stronger ion signals, mostly due to methylated benzenes. To verify whether the ion signal at mass 112 is due to monochlorobenzene, mass spectra were measured with two different laser wavelengths, 266 and 269.8 nm. Although the overall mass spectrum did not change strongly, the peak at mass 112 disappeared at 266 nm [see the inset in Fig. 9(b)]. In addition, the corresponding  $^{37}\text{Cl}_1\text{C}_6\text{H}_5$  peak at mass 114 u and the  $^{35}\text{Cl}_1^{13}\text{C}_1\text{C}_5\text{H}_5$  peak at mass 113 also disappeared at 266 nm. Hence the isotope pattern and wavelength dependence clearly prove the identity of the mass 112 peak. Using 269.8 nm, the sensitivity for monochlorobenzene improves to 25 pptv, whereas with 266 nm it is only 2 ppbv. From high-resolution GC/MS measurements, one knows that the average concentration is about 100 pptv and therefore below the detection limit for 266 nm laser ionization.

The mass spectra were taken within a few seconds without any sample clean-up, preparation, or preconcentration, demonstrating that resonant laser MS is appropriate for the fast control of pollutants during combustion processes on a large industrial scale. Time-resolved measurements of monochlorobenzene revealed that even for these large-scale processes, concentrations of pollutants (e.g. of polycyclic and substituted aromatic compounds) may be subject to fast fluctuations on a time-scale of seconds. The spectrum in Fig. 9(b) is one out of a fast cycle of laser MS experiments, which showed this temporal behavior.

## DRAWBACKS OF RESONANT LASER MASS SPECTROMETRY AND APPROACHES TO OVERCOMING THEM

As for most analytical techniques, there are also restrictions on resonant laser MS. They mostly arise from the particular photophysical behavior of some molecular species. The main problems for the most reasonable resonant laser ionization process (i.e. one color, nanosecond two-photon ionization) are illustrated in Fig. 10. While problems (a), (b) and (c) are due to unfavorable energies or molecular structure (i.e. case (c)) of the intermediate state or ion ground state, problem (d) is caused by fast intramolecular dynamic processes.

There are two ways to overcome problems (a) and (c). If a reduced selectivity of the ionization (due to a high density of states) is acceptable, a higher electronic or vibronic state may be chosen as an intermediate state. In case (a), where the intermediate state energy is too small, a higher electronic state (which fortunately often is subject to a larger absorption cross-section, such as the  $S_2$  state of aromatic compounds) has to be chosen. In case (c), where small Franck–Condon factors result in inefficient ionization, the excitation of an appropriate vibrational mode in the first excited electronic state (involving appropriate molecular structure changes) might help. The second way to cope with problems (a) and (c) is two-color ionization using two separate lasers. In most cases the second laser does not need to be tunable, but should supply photon energies further in the UV than the first laser. Often tunable lasers are pumped by fixed frequency lasers (e.g. excimer or YAG lasers) which supply photons of the necessary wavelength.

Case (b) is caused by too large an intermediate state energy. The real problem is the availability of tunable laser wavelengths. With frequency doubling in non-linear optics, tunable UV laser light down to about 200 nm can be generated. If the first intermediate state lies at higher energies (which is the case for several

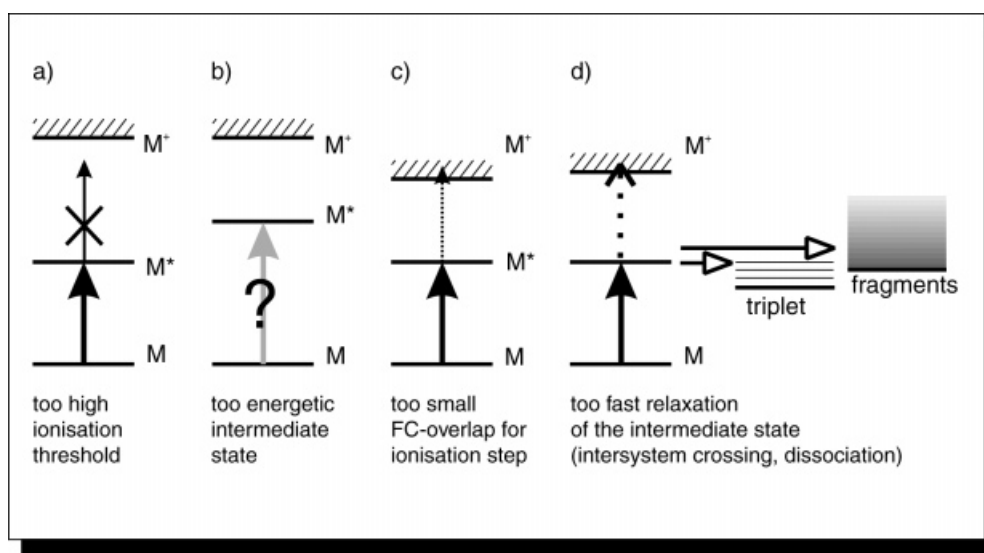


**Figure 10.** Four cases where one-color (1 + 1) two-photon ionization with nanosecond pulse lasers (the most reasonable realization of resonance-enhanced multiphoton ionisation) does not work (a, b) or is subject to strongly reduced efficiency (c, d). Increasing laser intensity may result in multiphoton processes of higher order (allowing ionization in case (a) or (b)) or in higher efficiency ((c),(d)) but mostly induces multiphoton absorption of the molecular ions causing more or less strong fragmentation. FC = Franck–Condon.

small molecules, alkanes, etc.; see Fig. 1), multiphoton absorption to this intermediate state (corresponding to an  $(n + m)$ -multiphoton ionization) has to be involved. For instance, CO is efficiently ionized by  $(2 + 1)$  MPI with a laser wavelength of 230 nm; even methanol can be ionized by  $(3 + 1)$  MPI at 457 nm, but with reduced sensitivity.

Cases (a), (b) and (c) become much less problematic if only semi-selective ionization of types of molecules (and not of single molecular species) is wanted. In this case, fixed-frequency lasers with sufficiently short wavelengths can be used. The most typical example is the wavelength of 266 nm (fourth harmonic of an Nd:YAG laser) at which most polycyclic and methylated aromatics are efficiently ionized. Excimer lasers also are well adapted for fixed-frequency, quasi-resonant laser ionization, e.g. the KrF laser emitting at 248 nm and the ArF laser at 193 nm.

In contrast to cases (a), (b) and (c) in Fig. 10, case (d) is not attributed to an energetic or structural problem but to a dynamic one. Fast relaxation processes empty the population of the intermediate state before secondary absorption into the ionization continuum can take place. Choosing a different intermediate state is usually not a solution since it is improbable that higher electronic states will show considerably longer lifetimes. One elegant way to overcome these short lifetimes is to perform the ionization step on an even shorter time-scale. Since

femtosecond lasers are commercially available, this is not just a hypothetical but a practical solution of the problem. In Fig. 11, two examples are displayed where nanosecond and femtosecond laser ionization are compared. The molecular species investigated in Fig. 11 are representative of molecules which are especially known for their very fast and efficient dissociation from electronically excited states, namely organometallic and nitroaromatic compounds.

In Fig. 11, diphenylmercury was studied by nano- and femtosecond excitation.<sup>43</sup> Wavelengths between 250 and 265 nm are available for both experiments. It is obvious that for nanosecond excitation no signal at the molecular mass is detectable, but strong peaks due to small fragments appear; these fragment ions are caused by primary ejection of the metal atom and secondary fragmentation of the phenyl group. In contrast to the nanosecond spectrum, at femtosecond excitation the molecular ion represents the dominant mass peak with only one further fragment ion (which is due to ejection of phenylmercury). On the right side of Fig. 11, nitrotoluene has been ionized by nanosecond and femtosecond laser light.<sup>44</sup> In the nanosecond mass spectrum,  $\text{NO}^+$  appears nearly exclusively. The inset illustrates the ionization pathway for this fragmentation. Fast dissociation of the neutral intermediate state results in neutral NO fragments, which (more or less accidentally) are ionized by 226 nm light very efficiently. No parent ion can

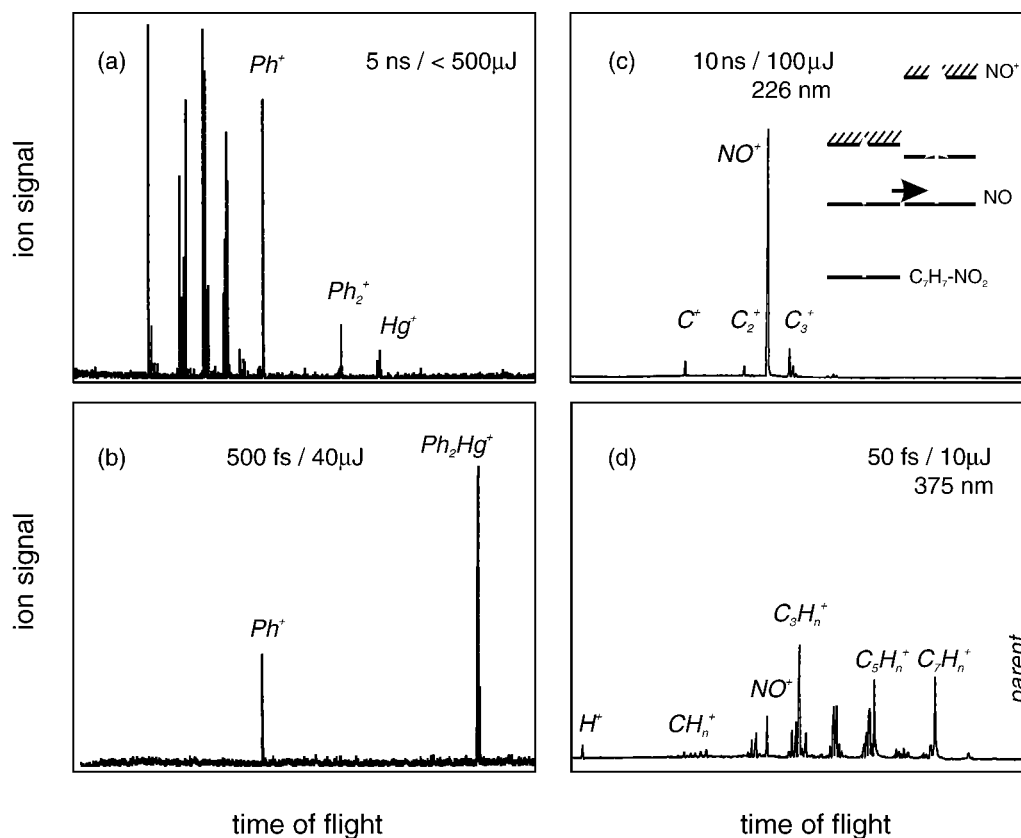


**Figure 11.** Ionization with very short pulse lasers. Left: laser mass spectra of diphenylmercury ionized by nanosecond (a) and by sub-picosecond (b) laser pulses (laser wavelength 250–265 nm). Reprinted from C. Weickhardt, C. Grun, J. Grotemeyer, *Eur. Mass Spectrom.* **4**, 239–244 (1998) with permission of IM Publications, Chichester. Right: laser mass spectra of nitrotoluene ionized by nanosecond (c) and by femtosecond (d) laser pulses. Reprinted from K. W. D. Ledingham *et al.*, *Rapid Commun. Mass Spectrom.* **9**, 1522–1527 (1995) with permission of John Wiley & Sons, Chichester. The high  $\text{NO}^+$  signal in spectrum (c) is due to a secondary multiphoton ionization of neutral NO fragments. A similar process is inducing the  $\text{Hg}^+$  signal in spectrum (a). It is obvious that ionization with ultra-short laser pulses is able to solve problem (d) in Fig. 10. In favorable cases, nanosecond laser ionization is able to produce fragment ions which are typical for molecular classes.

be detected at all. In contrast with this spectrum, the femtosecond mass spectrum clearly reveals a parent ion (and thus allows its identification), although dominant fragmentation could not be avoided even for laser pulses as short as 50 fs.

In Fig. 12, the resonant laser ionization of dibenzofuran, which is a textbook example including cases (a), (c) and (d) in Fig. 10, is displayed.<sup>45</sup> As shown in the excitation scheme, resonant excitation of the intermediate state with 312 nm radiation (from a frequency-doubled, Nd:YAG laser-pumped dye laser) does not allow the ionization threshold to be reached with a second 312 nm photon (case (a), Fig. 10). Two-color excitation with a 312 and a 266 nm photon should allow ionization from an energetic point of view. However, a very low efficiency is observed for this excitation scheme. The reason (see the experiment discussed below) is fast relaxation to the nearby triplet state (case (d), Fig. 10). Since this relaxation process is

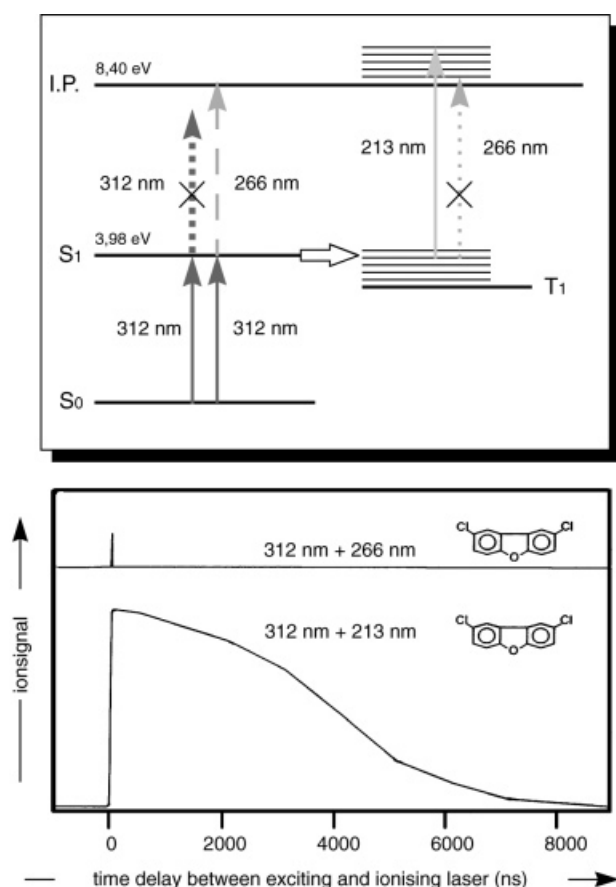


**Figure 12.** Two-color resonant laser ionization. (a) Scheme of two-color ionization of dichloro-dibenzofuran: resonant excitation of the  $S_1$  intermediate state by 312 nm (a second 312 nm photon does not reach the ionization continuum: case (a), Fig. 10). Also, a second 266 nm photon does not induce efficient ionization owing to fast energy relaxation to the vibrationally excited triplet state (intersystem crossing; see case (d), Fig. 10). The 266 nm photon does not ionize the vibrationally excited triplet state either (although energetically allowed) owing to very small Franck–Condon factors (case (c), Fig. 10). This problem is solved by a 213 nm photon. (b) Illustration of this processes by a 312 + 266 nm and a 312 + 213 nm ionization with temporal delay of first and second photons. Efficient ionization only at short delay times is a hint of fast relaxation processes (e.g. to the triplet state); the efficient ionization even at long delay times indicates that now the triplet state is efficiently ionized also. See also Ref. 45.

isoenergetic in the isolated gas phase, absorption of a 266 nm photon should still be able to ionize the molecule. However, since the triplet state  $T_1$  is energetically lowered in comparison with the first excited singlet state  $S_1$ , this relaxation leads to a vibrationally excited triplet state. Therefore, the vibrational wavefunctions of the initial and final states of the transition  $I.P. \leftarrow T_1$  show a very small overlap (FC factors) (case (c), Fig. 10). This can be improved by an even shorter wavelength of the second photon thus reaching higher vibrational levels of the molecular ion. Good results have been achieved with the fifth harmonic of an Nd:YAG laser at 213 nm.

In the lower part of Fig. 10, an experiment is shown which proves this argument. In this experiment, a primary laser with 312 nm and secondary laser with 266 or 213 nm were delayed in time. Using 266 nm as the wavelength of the second laser, the maximum ion signal is small and vanishes after very short delay times in the range of the laser pulse length (10 ns). This indicates that the short lifetime of the intermediate  $S_1$  state is the reason for low ionization efficiency at 266 nm (ionization of the triplet  $T_1$  by 266 nm is not efficient). When 213 nm is chosen as the wavelength of the second laser, an intensity increase of more than a factor of five is observed. This intensity stays nearly unchanged for delay times in the microsecond range corresponding to typical triplet lifetimes. This second result indeed proves that even for fast intramolecular dynamic processes, two-color, two-photon ionization is an optimum ionization scheme. This is true as long as dissociation processes are not active and destroy molecular mass information.

In addition to two-color ionization, fixed-frequency ionization (reduced selectivity), femtosecond excitation or  $(n + m)$  multiphoton ionization (with  $n > 1$ ), some other laser-induced gas-phase ionization techniques should be mentioned. One is laser-induced vacuum UV (VUV), which is generated by focusing laser light into a gas cell filled with noble gas (e.g. Kr, Ar). The very useful wavelength of 118 nm for semi-selective single photon ionization is generated with the third harmonic of an Nd:YAG laser at 355 nm (for general information about laser techniques for spectroscopy, see Ref. 46 and references cited therein). At 118 nm most larger molecules are ionized while the ionization threshold of those small molecules which represent by far the main part of air samples lies above this energy. A further advantage of laser-induced VUV ionization is that it is not affected by the problems addressed in Fig. 10 (at too small excess energies above the ionization threshold, Franck–Condon factors might be small in some cases). Owing to small photon numbers per laser pulse, the sensitivity is reduced in comparison with resonant laser ionization.

Similar arguments concerning sensitivity and the problems addressed in Fig. 10 are valid for laser-induced electron ionization.<sup>47</sup> Electron ionization is very useful as a non-selective ionization method delivering a general survey about the main components of a gas sample. Even more useful is the combination of electron ionization and resonant laser ionization in the same ion source. This combination allows one to obtain the above-mentioned survey information and also very selective information (e.g. special trace compounds) within one mass spectrum. In Fig. 13, a possible arrangement to achieve such a parallel ionization is displayed. A laser beam is coupled into

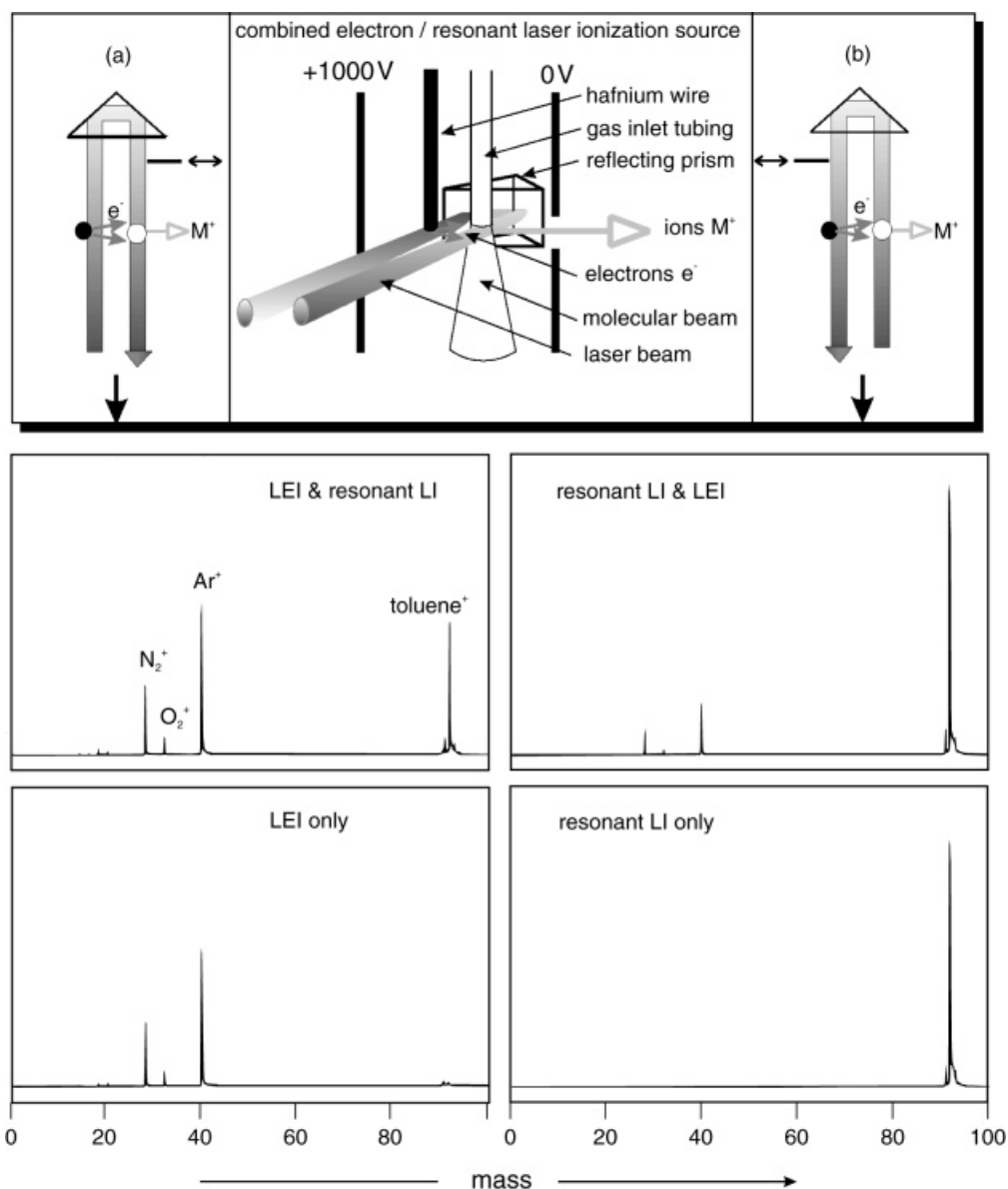


**Figure 13.** The combination of electron ionization and resonance-enhanced multiphoton ionization as an example of the flexibility of laser-induced ionization. Laser-induced electron ionization (LEI) is achieved by a metal (with low work function, e.g. hafnium) wire tip which is hit by the laser and then emits a burst of electrons. Resonant laser ionization (resonant LI) takes place in a molecular beam just at the end of a thin tube. The combination of LEI and resonant LI is achieved by reflecting the laser beam back into the ion source. Two arrangements are realized: first LEI, then resonant LI (a), and first resonant LI, then LEI (b). Four mass spectra of an air–argon gas mixture with traces of toluene are shown. For both arrangements, the reflected laser beam can be blocked giving rise to singly LEI or singly resonant LI mass spectra. The effects of both ionization processes are obvious, and also the fact that ions from two different ionization processes appear in a single mass spectrum. H. Nagel, M. Grandl, U. Boesl, unpublished results.

a molecular beam just below the end of a gas inlet tubing and then is reflected by a prism which additionally causes a parallel shift. Thus, the laser beam enters the ion optics a second time and produces photoelectrons from a wire with a low work function (e.g. hafnium). By applying a pulsed negative voltage of about 70–100 V with respect to the gas inlet tubing, the electrons are accelerated towards the molecular beam and cause additional ionization. Both processes can be controlled separately and optimized for the actual analytical situations. To check the effect of both ionization processes, the direction of the laser beam can be turned, hitting the wire first and passing under the gas inlet tubing afterwards. In both cases, the laser beam can be blocked after the first ionization process (resonant laser ionization or electron ionization,

respectively). The mass spectra due to these four different ionization arrangements are shown at the bottom of Fig. 13. A mixture of air and argon with traces of toluene serves as illustrative gas sample. It is shown how each ionization process can be switched on or off separately or can be combined. This switching may take place within 0.1 s. In addition, the different effects of the two ionization methods is obvious: the main gas components appear upon electron ionization and selected trace compounds occur on resonant laser ionization.

Finally, there exists the possibility of performing tandem mass spectrometry with laser excitation and reflectron time-of-flight mass analyzers without substantial additional hardware. Tandem mass spectrometry is one of the most important conventional techniques of trace

analysis; however, the instrumental effort is large. Reflectron time-of-flight mass analyzers have an intrinsic second point of mass selectivity (namely the so-called space-focus of the ion source). Here, secondary laser excitation allows mass-selective fragmentation.<sup>34,48</sup> In addition, laser excitation may induce metastable decay of molecular ions; in this case, the special features of reflectron time-of-flight mass analyzers with respect to metastable decay in the field-free region<sup>39,49,50</sup> (sometimes called post-source decay) allow tandem mass spectrometry with low additional effort, again. Whichever method is used, if isobaric molecular species have different secondary mass spectra, then this is another method of selective laser-induced mass spectrometry, which may compensate for reduced selectivity of the ionization step (e.g. due to fixed-frequency, medium-resolution or single-photon ionization). The necessary double laser pulses with adequate separation (e.g. some tens of  $\mu\text{s}$ ) are available from some commercial Nd:YAG lasers by switching the quality of the laser resonator twice during one flash lamp pulse.

## CONCLUSION

The typical applications described above demonstrate that resonant laser mass spectrometry is valuable in actual

analytical problems which cannot be solved by conventional techniques of trace analysis. This involves fast, rapidly changing combustion processes (e.g. combustion engines), fast on-site analysis of single chemical species (e.g. the PAH load of aerosols, pollutants due to chemical accidents), on-line analysis of trace compounds which may act as indicators for highly poisonous substances (e.g. polychlorinated dioxins) with far lower concentrations or the fast measurement of whole chemical patterns (with single species selectivity and not overall sum values such as the 'total hydrocarbon content') to identify and control the state of technical incinerators or even chemical plants.

This tendency will be supported and, hopefully, accelerated by new generations of lasers. Thus, very small but nevertheless powerful Nd:YAG lasers now are commercially available, in addition to reliable, small excimer lasers with high repetition rates of up to 500 Hz and of reasonable cost. This development is completed by new tunable lasers (e.g. OPO lasers) with good wavelength resolution of a few wavenumbers and very small size. However, also on the side of the mass spectrometer and vacuum system, a considerable reduction in size is possible. To summarize, mobile instruments equipped for rough, every-day environmental conditions in industry (maybe at the expense of ultra-high selectivity or even sensitivity, but not of rapidity) are one goal for the future development of resonant laser mass spectrometry.

## REFERENCES

- Lubman D. *Lasers in Mass Spectrometry*. New York: Oxford University Press, 1990.
- Vertes A, Gijbels R, Adams F. *Laser Ionization Mass Analysis*. New York: John Wiley & Sons, 1993.
- Cotter R. *Anal. Chem.* 1984; **56**: 485A.
- Lubman D. *Anal. Chem.* 1984; **56**: 1256A.
- Lin S, Fujimura Y, Neusser H, Schlag E. *Multiphoton Spectroscopy of Molecules*. Orlando, FL: Academic Press, 1984.
- Letokhov V. *Laser Photoionization Spectroscopy*. Orlando, FL: Academic Press, 1987.
- Boesl U. *J. Phys. Chem.* 1991; **95**: 2949.
- Boesl U. In *Encyclopedia of Spectroscopy and Spectrometry*, McNeil C (ed.). New York: Academic Press, in press.
- Johnson P. *Appl. Opt.* 1980; **19**: 3920.
- Boesl U, Neusser H, Schlag E. *J. Chem. Phys.* 1980; **72**: 4327.
- Bernstein R. *J. Phys. Chem.* 1982; **86**: 1178.
- Lubman D, Kronick M. *Anal. Chem.* 1982; **54**: 660.
- Gedanken A, Robin M, Kuebler N. *J. Phys. Chem.* 1982; **86**: 4096.
- Gobeli D, Yang J, El-Sayed M. *Chem. Rev.* 1985; **85**: 529.
- Grotemeyer J, Schlag E. *Angew. Chem., Int. Ed. Engl.* 1988; **27**: 447.
- Boesl U, Weinkauff R, Weickhardt C, Schlag E. *Int. J. Mass Spectrom. Ion Processes* 1994; **131**: 87.
- Zenobi R. *Int. J. Mass Spectrom. Ion Processes* 1995; **145**: 51.
- Zenobi R, Zhan Q, Voumard P. *Mikrochim. Acta* 1996; **124**: 273.
- Ledingham K, Singhal R. *Int. J. Mass Spectrom. Ion Processes* 1997; **163**: 149.
- Haefliger O, Zenobi R. *Anal. Chem.* 1998; **70**: 2660.
- Boesl U, Heger H, Zimmermann R, Püffel P, Nagel H. In *Encyclopedia of Chemical Analysis*, Meyers RA (ed.). New York: John Wiley & Sons, in press.
- Jaffé H, Orchin M. *Theory and Applications of Ultraviolet Spectroscopy*. New York: John Wiley & Sons, 1962.
- Dietz TG, Duncan MA, Livermann MG, Smalley RE. *J. Chem. Phys.* 1980; **73**: 4816.
- Amirav A, Even U, Jortner J. *Anal. Chem.* 1982; 1666.
- Hayes J. *Chem. Rev.* 1987; **87**: 745, 760.
- Zimmermann R, Lerner C, Schramm K, Kettrup A, Boesl U. *Eur. Mass Spectrom.* 1995; **1**: 341.
- Oser H, Thanner R, Grotheer H. *Combust. Sci. Technol.* 1996; **116/117**: 567.
- Castaldi M, Senkan S. *J. Air Waste Manage. Assoc.* 1998; **48**: 77.
- Heger H, Zimmermann R, Dorfner R, Beckmann M, Griebel H, Kettrup A, Boesl U. *Anal. Chem.* 1999; **71**: 46.
- Guilhaus M. *J. Mass Spectrom.* 1995; **30**: 1519.
- Schlag E (ed.). *Time-of-Flight Mass Spectrometry and its Applications*. *Int. J. Mass Spectrom. Ion Processes* 1994; **131**.
- Wiley W, McLaren I. *Rev. Sci. Instrum.* 1955; **26**: 1150.
- Mamyrin B, Karataev V, Shmikk D, Zagulin V. *Sov. Phys. JETP* 1973; **37**: 45.
- Boesl U, Weinkauff R, Schlag E. *Int. J. Mass Spectrom. Ion Processes* 1992; **112**: 121.
- Tanada T, Valezquez, Hemmi N, Cool T. *Ber. Bunsen-Ges. Phys. Chem.* 1993; **97**: 1516.
- Püffel P, Thiel W, Frey R, Boesl U. *SAE Tech. Pap. Ser.* 1998; No. 982438: 1.
- Püffel P, Boesl U. *VDI Ber.* 1999; **1470**: 215.
- Zhan Q, Voumard P, Zenobi R. *Rapid Commun. Mass Spectrom.* 1995; **9**: 119.
- Spengler B. *J. Mass Spectrom.* 1997; **32**: 1019.
- deHoffmann E. *J. Mass Spectrom.* 1996; **31**: 129.
- Blumenstock M, Zimmermann R, Schramm K, Kaune A, Nikolai U, Lenoir D, Kettrup A. *J. Anal. Appl. Pyrol.* 1999; **49**: 179.
- Zimmermann R, Heger H, Blumenstock M, Dorfner R, Schramm K, Boesl U, Kettrup A. *Rapid Commun. Mass Spectrom.* 1999; **13**: 307.
- Weickhardt C, Grun C, Grotemeyer J. *Eur. Mass Spectrom.* 1998; **4**: 239.

44. Ledingham K, Kilic H, Kosmidis C, Deas R, Marshall A, McCanny T, Singhal R, Langley A, Shaikh W. *Rapid Commun. Mass Spectrom.* 1995; **9**: 1522.
45. Zimmermann R, Lenoir D, Kettrup A, Nagel H, Boesl U. In *27th Symposium on Combustion*. The Combustion Institute, Pittsburgh: 1996; D2859–2868.
46. Demtröder W. *Laser Spectroscopy* (2nd edn). Berlin: Springer, 1996.
47. Rohwer E, Beavis R, Köster C, Lindner J, Grotemeyer J, Schlag E. *Z. Naturforsch., Teil A* 1988; **43**: 1151.
48. Boesl U, Weinkauff R, Walter K, Weickhardt C, Schlag E. *J. Phys. Chem.* 1990; **94**: 8567.
49. Boesl U, Neusser HJ, Weinkauff R, Schlag E. *J. Phys. Chem.* 1982; **86**: 4857.
50. Ioanoviciu D, Yefchak G, Enke C. *Int. J. Mass Spectrom. Ion Processes* 1991; **104**: 83.